Molecular Insights into Functional Differences Between *mcr-3*- and *mcr-1*-Mediated Colistin Resistance

Hui Li,[a,b] Lu Yang,[a] Zhihai Liu,[a] Wenjuan Yin,[a] Dejun Liu,[a] Yingbo Shen,[a] Timothy Walsh,[c] Bing Shao,[a,b#] Yang Wang[d#]

[a]Beijing Advanced Innovation Center for Food Nutrition and Human Health, College of Veterinary Medicine, China Agricultural University, Beijing, P. R. China.

[b]Beijing Key Laboratory of Diagnostic and Traceability Technologies for Food Poisoning, Beijing Center for Disease Prevention and Control, Beijing, P. R. China.

[c]Department of Medical Microbiology and Infectious Disease, Division of Infection and Immunity, Cardiff University, Cardiff, UK.

[d]Beijing Key Laboratory of Detection Technology for Animal-Derived Food Safety, China Agricultural University, Beijing, P. R. China.

H.L. and L.Y. contributed equally to this work.

#Address correspondence to Bing Shao shaobingch@sina.com or Yang Wang wangyang@cau.edu.cn

Running title: Functional Differences Between *mcr-3* and *mcr-1*

ABSTRACT

The global emergence of plasmid-mediated colistin resistance genes *mcr-1* and *mcr-3* has threatened the role of the "last resort" drug colistin in the defense against infections caused by multidrug-resistant Gram-negative bacteria. However, functional differences between these two genes in mediating colistin resistance remains poorly understood. Protein sequence alignment of MCR-3 and MCR-1 was therefore conducted in Clustal Omega to identify sequence divergence. The molecular recognition of lipid A head group phosphatidylethanolamine and MCR-3 enzyme was studied by homology modeling and molecular docking, with the catalytic mechanism of MCR-3 also being explored. Thr277 in MCR-3 was validated as the key amino acid residue responsible for the catalytic reaction using site-directed mutagenesis and was shown to act as a nucleophile. Lipid A modification induced by the MCR-3 and MCR-1 enzymes was confirmed by electrospray ionization time-of-flight mass spectrometry. Far-UV circular dichroism spectra of the MCR-3 and MCR-1 enzymes suggested that MCR-3 was more thermostable than MCR-1, with a melting temperature of 66.19°C compared with 61.14°C for MCR-1. These data provided molecular insight into the functional differences between *mcr-3* and *mcr-1* in conferring colistin resistance.

Keywords: *mcr-3*, *mcr-1*, colistin resistance, homology modeling, phosphatidylethanolamine

INTRODUCTION

The emergence of multidrug-resistant Gram-negative pathogenic bacteria represents one of the greatest global public health threats to date (1). Colistin is considered the last line of defense against many of these clinical multidrug-resistant microorganisms (2, 3). The antibacterial activity of colistin occurs as a result of an electrostatic interaction between the α,γ-diaminobutyric acid residue of the positively-charged colistin and the phosphate groups of the negatively-charged lipid A membrane. This destabilizes the lipopolysaccharide, consequently increasing the permeability of the bacterial membrane. The colistin molecule can then insert itself into the bacterial cell (2, 4). Modification of lipid A at the 1′ and 4′ head group positions with phosphoethanolamine (PEA) or 4-amino-arabinose masks the negatively-charged phosphate groups on the bacterial surface, thereby preventing the interaction with cationic antimicrobial peptides such as colistin and polymyxin B (5). Plasmid-mediated mobilized colistin resistance (MCR) enzymes, encoded by *mcr-1–5* (6-10), are members of the PEA transferase family of proteins that decorate the lipid A head groups of lipopolysaccharide with PEA, thereby conferring colistin resistance.

Recently, we described a new transferable plasmid-borne colistin resistance gene, *mcr-3*, in an *Escherichia coli* isolate from pig feces (7). Subsequent epidemiological studies have shown that, similar to *mcr-1*, *mcr-3* is widespread amongst various species of *Enterobacteriaceae* and *Aeromonas* (11-14). Considering the spread and prevalence of these two genes and their potential harm with regard to drug-resistant bacterial infections (15-17), this study aimed to provide molecular insights into the functional differences between *mcr-3* and *mcr-1*. Furthermore, the molecular mechanism underlying substrate binding by *mcr-3*

remains to be elucidated, and there is virtually no research deciphering its role in mediating colistin resistance. To address these issues, we carried out homology modeling and examined the molecular docking of MCR-3 with the substrate, L-α-phosphatidylethanolamine (L-αPEA), from *E. coli*. Identifying the catalytic mechanism and possible binding sites would aid in subsequent characterization of their biological characteristics. We also expressed and purified MCR-1 and MCR-3 and determined the thermal stability and secondary structure of these two lipid A PEA transferases. These functional comparisons showed that MCR-3 was more thermostable than MCR-1.

MATERIALS AND METHODS

Strains and plasmid construction

mcr-3 was cloned from the genomic DNA of *E. coli* plasmid pWJ1 by PCR using forward (5′-GGGAATTCCATATGATGCCTTCCCTTATAAAAAT-3′) and reverse (5′-AAGGAAAAAAGCGGCCGCTTATTGAACATTACGACATTGAC-3′) primers incorporating NdeI and NotI restriction sites at the N- and C-termini of the coding region, respectively. The resulting PCR products were digested with the corresponding restriction enzymes and ligated into expression vector pET28a, generating pET28a-*mcr-3*. *mcr-1* was then PCR-amplified from *E. coli* strain SHP45 genomic DNA using forward (5′-CATGCCATGGTGATGATGCAGCATACTTCTGTGTGGTACCGACG-3′) and reverse (5′-CAAAGACCGCACCGCATTCATCCGCCTCGAGCGG-3′) primers and cloned into plasmid pET28a to generate a high-copy expression vector with an N-terminal hexa-histidine tag (pET28a-*mcr-1*). The resulting recombinant MCR-3 and MCR-1 proteins contained a

tobacco etch virus protease cleavage site followed by a 6×His tag at the N terminus. The calculated molecular masses of both the recombinant and cleaved monomeric MCR-3 and MCR-1 proteins were ~60 kDa.

Expression and purification of full-length MCR-3 and MCR-1

For overexpression analyses, pET28a-*mcr-3* and pET28a-*mcr-1* were individually transformed into *E. coli* BL21 (DE3) pLysS chemically-competent cells. The transformants were then cultured in Luria Bertani (LB) medium supplemented with 50 μg/ml kanamycin at 37 °C with shaking for 3–4 h, or to an optical density at 600 nm (OD_{600}) of 0.5–0.6. Protein expression was induced by the addition of 0.4 mM isopropyl-β-D-thiogalactopyranoside and incubation at 18 °C for a further 20 h. Cells were harvested by centrifugation at 10,000 × *g* for 10 min at 4 °C and then re-suspended in lysis buffer (50 mM sodium phosphate buffer, pH 8.0, containing 300 mM sodium chloride and 10 mM imidazole). Cell debris was removed by centrifugation at 12,000 × *g* for 20 min at 4 °C, and membranes were collected by further ultracentrifugation of the supernatant at 100,000 × *g* for 1 h at 4 °C using an ultracentrifuge (Optima XE-100; Beckman Coulter, Brea, CA, USA). The resulting pellet was homogenized in phosphate-buffered saline containing 1% *n*-dodecyl-β-D-maltoside (DDM) and solubilized for 2 h at 4 °C on a rotational shaker at 50 rpm.

To purify the full-length MCR-1 and MCR-3, protein-containing supernatant was applied to a Ni-NTA Superflow resin column (Qiagen, Hilden, Germany) equilibrated with binding buffer (50 mM sodium phosphate, pH 7.5, 300 mM NaCl, 10 mM imidazole). The unbound protein was washed from the column using washing buffer (50 mM sodium phosphate, pH 7.5, 300 mM NaCl, 20 mM imidazole), and the bound protein was eluted from the column

using elution buffer (50 mM sodium phosphate, pH 7.5, 300 mM NaCl, 200 mM imidazole, 0.05% (w/v) DDM). The eluent fractions were pooled and concentrated using a Vivaspin 20 centrifugal concentrator (MWCO 10 K; Sartorius, Göttingen, Germany) to a final concentration of 5–10 mg/ml, as determined by the absorbance at 280 nm using a NanoDrop 2000c spectrophotometer.

Isolation and mass spectrometry of lipid A

The construction of *E. coli* strains W3110 (pUC19), W3110 (pUC19-*mcr-3*), and W3110 (pUC19-*mcr-1*) was described in our previous research (6, 7). Bacterial cultures (200 ml) were incubated overnight in LB broth at 37 °C, and then cells were harvested by centrifugation at 10,000 × *g* for 10 min. Lipid A was isolated by mild acidic hydrolysis according to the method described previously by Hankins *et al*. (18). Lipid A was analyzed using electrospray ionization quadrupole time-of-flight mass spectrometry (ESI-TOF/MS) (Waters Synapt HR-MS, Milford, USA) in the negative-ion mode. The ESI-TOF/MS settings were as follows: capillary voltage, 3.0 kV; sampling cone voltage, 30 V; source temperature, 100 °C; desolvation temperature, 500 °C; and desolvation gas (N_2), 600 l/h.

Circular dichroism (CD) spectroscopy

The far-UV spectra of MCR-1 and MCR-3 were measured at 20 °C on a CD spectrophotometer (Jasco J-810, Tokyo, Japan) using a 1-mm path-length quartz cuvette. The protein sample was diluted to a concentration of 0.2 mg/ml in 5 mM sodium phosphate (pH 7.0). CD data were collected every 1 nm using a 1-nm bandwidth in the 185–260-nm wavelength region using an integration time of 1 s per step. Temperature-dependent CD analysis was carried out at 220 nm with a temperature range of 10–90 °C and a rate of

1 °C/min to determine the melting temperature (Tm). The resulting spectra represented the average of three accumulations and were buffer-baseline corrected with the signal-to-noise ratio improved using the Savitzky-Golay method with a minimum convolution width of 5 data points. Analysis was conducted using Spectra Analysis software (version 1.53.07 for Windows 95/NT; JASCO Corp., Tokyo, Japan).

Molecular docking

To provide an overview of full-length MCR-3, structural modeling was performed using two approaches: the SWISS-MODEL workspace and the Modweb server (19, 20). Sequence alignment of MCR-1, MCR-3, and EptA was conducted using Clustal Omega (http://www.ebi.ac.uk/Tools/msa/clustalo/). The crystal structure of EptA (PDB ID: 5FGN) was used for modeling by comparing the E-value and the structure total score. The EptA structure was embedded into L-αPEA from *E. coli* using the Swiss-Model automated homology-modeling server (https://swissmodel.expasy.org/). PROCHECK and ERRAT were used to evaluate the optimized model protein structure. A Ramachandran plot was used to illustrate the degree of rotation of the bonds between the α-carbon atoms and the carbonyl carbon atoms of the peptide bond in a peptide or peptide structure of a protein. The degree of rotation of the bond between the α-carbon atom and the nitrogen atom was mainly used to indicate permitted and impermissible conformations of amino acid residues. The structure of the protein after modeling was studied to further discuss the rationality of the model and analyze the catalytic structure of MCR-3.

The interaction between the ligand and the MCR-3 protein structure, determined by homology modeling, was investigated using AutoDock Tools 1.5.6, which generated the

pdbqt files used for molecular docking analysis. Molecular docking was completed using the MolDesigner molecular simulation platform of AutoDock Vina (21). If the molecular docking results produced unreasonable atomic contacts in the spatial structure, energy-optimized methods were used to release these forces to stabilize the structure.

Construction of *mcr-3* site-directed mutants

To test the role of Thr277 in MCR-3, two different substitution-inducing mutations (Thr277Ala and Thr277Ser) were introduced into *mcr-3* in pUC19-*mcr-3* using a QuikChange Lightning Site-Directed Mutagenesis Kit (Agilent Technologies, Santa Clara, CA, USA) as per the manufacturer's protocol using primers Thr277Ala-F (5′-TCGTGTGGGACTGCAGCCGCTGTATCCGTCCCC-3′) and Thr277Ala-R (5′-GGGGACGGATACAGCGGCTGCAGTCCCACACGA-3′), and Thr277Ser-F (5′-TCGTGTGGGACTGCAAGCGCTGTATCCGTCCCC-3′) and Thr277Ser-R (5′-GGGGACGGATACAGCGCTTGCAGTCCCACACGA-3′), respectively. These primers introduced an ACC (coding for threonine) to GCC (coding for alanine) or AGC (coding for serine) mutation at residue 277 of MCR-3. Recombinant plasmids containing wild-type *mcr-3* or each of the two mutations (Thr277Ala and Thr277Ser) were then transformed into host *E. coli* strain DH5α. Sequencing of the complete *mcr-3* genes from each of the transformants was conducted to ensure no extraneous mutations occurred. Minimum inhibitory concentrations (MICs) of colistin and polymyxin for *E. coli* DH5α, DH5α (pUC19), DH5α (pUC19-*mcr-3*), and each of the site-directed mutants were measured by the broth microdilution method according to the Clinical and Laboratory Standards Institute guidelines (22).

168

169 **RESULTS AND DISCUSSION**

170 **Lipid A modification mediated by *mcr-3* and *mcr-1* confirmed by ESI-TOF/MS**

171 *mcr-3* and *mcr-1* encode PEA transferases that mediate colistin resistance in a variety of
172 bacterial species, including *E. coli, Aeromonas veronii*, *Salmonella enterica* serovar
173 Typhimurium, *Klebsiella pneumoniae*, and *Citrobacter freundii* (12-14). In this study, lipid A
174 was extracted from recombinant *E. coli* strains W3110 (pUC19-*mcr-3*), *E. coli* W3110
175 (pUC19-*mcr-1*), and *E. coli* W3110 (pUC19) and the lipid spectra was analyzed by
176 ESI-TOF/MS. ESI-MS/MS spectra showed that lipid A from *E. coli* W3110 (pUC19) had a
177 prominent peak at *m/z* 1797.10 (Fig. 1A). Upon the addition of a PEA molecule (123 Da) to
178 the bis-phosphorylated hexa-acylated lipid A in both *E. coli* W3110 (pUC19-*mcr-1*) and
179 W3110 (pUC19-*mcr-3*), the peak shifted to *m/z* 1920 (i.e., 1797 + 123) (Fig. 1B, C). Previous
180 research has shown that MCR-1 can transfer PEA from phosphatidylethanolamine to the
181 negatively-charged phosphate groups of lipid A, resulting in decreased affinity for colistin (23,
182 24). The proposed lipid A modification catalyzed by MCR-3 is shown in Fig. 1D. Thus, we
183 confirmed that MCR-3, like MCR-1, could modify lipid A on the bacterial cell membrane,
184 thereby mediating colistin resistance.

185 **Comparison of the models of full-length MCR-3 and MCR-1**

186 Four proteins, EptA (PDB:5FGN), LptA (PDB:4KAY and 4KAV), and MCR-1
187 (PDB:5K4P), were aligned to select a template for homology modeling. In general, protein
188 crystals with higher total scores or E-values less than $1e^{-5}$ can be considered for use as
189 templates. Both the SWISS-MODEL workspace and the Modweb server automatically

selected full-length EptA as the template for homology modeling and returned similar modeling results (Table 1 and Fig. 2). Template 5FGN had the highest score with the target sequence, with a sequence identity of 39%. Templates 4KAY and 4KAV reached 44% sequence identity but the sequence coverage was only 60% (Table 1), indicating that they were missing part of the structure and were not suitable as templates for building a complete protein model. 5K4P only showed 35% sequence identity with MCR-3.

The structure of MCR-3 was composed of two folded domains: an N-terminal transmembrane (TM) domain and a C-terminal catalytic domain. The TM domain consisted of five membrane-spanning α-helices (residues 1–212) connected to the catalytic domain via a bridging helix (Fig. 3). There were multiple lysine and histidine residues on the membrane surface, and these basic amino acids could improve the stability of MCR-3 on the membrane to a certain extent. The soluble cytoplasmic domain had a similar structure to the hydrolase active site (5). The Zn^{2+} ions bound to the active site and formed tetrahedral coordination structures with Glu238, Thr277, Asp450, and His451, with distances of 1.9, 2.2, 2.0, and 1.9 Å, respectively. Thr277 was the key amino acid responsible for the catalytic reaction, acting as a nucleophile. In addition, disulfide bonds formed by five pairs of cysteines were distributed in this region, which stabilized the structure of the region as a whole. Furthermore, conserved residue Thr285 in the MCR-1 catalytic domain structure is believed to act as the acceptor for the PEA group during the transfer reaction (25-27). MCR-1 transfers PEA to lipid A, which is located in the nearby pocket consisting of Thr283, Ser284, Tyr287, Pro481, and Asn482 (28). It was demonstrated that a threonine residue (Thr285 for MCR-1 and Thr277 for MCR-3) in the catalytic domain played an important role in mediating colistin

212 resistance. The rationality of the MCR-3 protein homology modeling and the structural
213 integrity of the catalytic active center proved the reliability of the structure and could be used
214 for subsequent molecular docking analyses to explore the catalytic mechanism of MCR-3.

215 **Catalytic reaction mechanism of MCR-3 deciphered by molecular docking**

216 Prior to the catalytic transfer of PEA by MCR-3, the side-chain hydroxyls of the
217 catalytically-active Thr277 lose their hydrogen protons, forming oxyanions by nucleophilic
218 attack. In the MCR-3 model, the amino acid residues Glu111, His380, and His463 could
219 receive the hydrogen proton in the vicinity of the catalytic center. The distances between the
220 oxygen of Thr277 and the three residues were 5.3, 5.4, and 5.1 Å, respectively. It would be
221 difficult to directly transfer the proton from these spatial distances. However, there was a
222 water molecule between these three amino acids, which was not present in the catalytic center
223 of the general template crystal structure of EptA. The hydrogen protons of Thr277 are
224 therefore likely to be transferred by the water molecule to the three residues. The results of
225 molecular docking analysis showed that PEA could bind to the catalytically-active cavity of
226 MCR-3, with a binding energy of −7.1 kcal/mol. The main driving power of PEA binding
227 was the “head” hydrogen and the “tail” hydrophobicity (Fig. 4). The PEA moiety at the head
228 of L-αPEA formed a hydrogen bond network with Glu111, Thr277, Ala278, His451, and
229 His463. These hydrogen bonds would stabilize the PEA head in the catalytic center of the
230 MCR-3 enzyme, which would be favorable for the subsequent catalytic reaction. The alkyl
231 chain at the terminus of L-αPEA extended into the transmembrane region of the MCR-3
232 protein and formed strong hydrophobic bonds with the Ile84, Thr88, Val94, Asn103, Ile104,
233 Ala112, Tyr115, Leu116, Ile120, and Leu462 residues. This hydrophobic interaction would

234 enhance the stable binding of the PEA substrate to the active cavity of the MCR-3 enzyme.

235 We further analyzed the binding conformations and found that the distance between the
236 O1 of the L-α-PEA molecule and Zn^{2+} in the catalytic center was 2.7 Å, while the distance
237 between the P atom of the phosphoric acid group and the O atom of the Thr277 hydroxyl was
238 3.1 Å. This finding demonstrated that the two pairs of atoms might be separated by the
239 electrostatic interactions of the O1-Zn and P-O covalent bonds, respectively. It was also
240 noteworthy that the O2 of the terminal alkyl side chain in L-αPEA formed a hydrogen bond
241 with His463 at a distance of 2.2 Å, indicating that hydrogen protons on His463 might be
242 transferred to the O2 of L-αPEA. The P-O2 bond then broke to form a product. We
243 concluded that the hydrogen proton of Thr277 was likely to be transferred to the His463
244 residue via a water molecule. The protonated His463 could then provide hydrogen protons to
245 the alkyl chains at the ends of L-αPEA to complete the entire catalysis reaction.

246 Next, we speculated on the possible mechanism of the MCR-3-catalyzed reaction (Fig. 5).
247 The reaction was divided into two main steps: (1) the hydrogen protons on the
248 catalytically-active Thr277 side chain hydroxyls in MCR-3 were transferred to the nitrogen of
249 the His466 residue side chains via water molecules. Thr277 was further activated to become a
250 nucleophilic attacking group, and the protonated His463 residue was subsequently involved
251 in the reaction as a hydrogen proton donor. At the same time, the carboxylate of Glu238
252 would attract the carboxyl hydrogen proton of Asp321 to Glu238, leaving the catalytic center
253 electrically neutral. (2) During L-αPEA binding to the catalytically-active site, the O1 of the
254 phosphate group coordinates with Zn to form a coordinate covalent bond. P forms a covalent
255 bond with the hydroxyl oxygen of Thr277, and the covalently-linked bonds between the O2

256 in the terminal alkyl side chain and P were broken, forming the Thr-PEA complexes. The
257 Thr-PEA complex is a positively-charged group, which would result in a decrease in the
258 negative charge of the bacterial outer membrane, reducing the absorbance capacity of the
259 bacterium for positively-charged colistin, which in turn leads to bacterial resistance to
260 colistin.

261 **Mutation of Thr277 decreases MCR-3 function**

262 As Thr277 was considered to be the key amino acid responsible for the catalytic reaction,
263 mutation of this amino acid would be expected to decrease the functional abilities of MCR-3.
264 To test this hypothesis, we constructed two strains carrying plasmid pUC19-*mcr-3* containing
265 mutations within MCR-3 (Thr277Ala and Thr277Ser). We then measured the MICs of
266 colistin and polymyxin for these strains in comparison with the wild-type. The MIC of
267 colistin for the strain containing pUC19-*mcr-3* was 4.0 μg/ml, compared with 0.5 μg/ml for
268 the control strain containing empty plasmid (pUC19). The strain containing a Thr277Ala
269 substitution in MCR-3 had a colistin MIC similar to that of the control (0.5–1 μg/ml, Table 2),
270 while the Thr277Ser mutation resulted in a 4-fold decrease in the MICs of colistin and
271 polymyxin compared with the *E. coli* DH5α (pUC19-*mcr-3*) strain (Table 2). Taken together,
272 site-directed mutagenesis verified the importance of the Thr277 residue to the catalytic
273 activity of lipid A.

274 **MCR-3 shows greater thermostability than MCR-1**

275 In the absence of high-resolution structures, CD is the method of choice for providing
276 secondary structural information for proteins in solution (29). To explore the resistance
277 mechanism of the novel MCR-3 protein and compare its structure and function with MCR-1,

we expressed and purified the full-length MCR-3 protein. Characterization of the secondary structures of MCR-1 and MCR-3 was then achieved using CD spectra. The normalized CD spectra of MCR-1 and MCR-3 from 185–260 nm are shown in Fig. 6A. MCR-3 and MCR-1 were well-folded, structured proteins and presented similar structural properties with regard to α-helical and β-sheet content from the deconvolution. We also compared the thermal stability of MCR-3 and MCR-1 using temperature-dependent CD. As a result, melting temperatures of approximately 66.19 °C and 61.14 °C were obtained for MCR-3 and MCR-1, respectively. The CD results showed clear differences in the thermal stabilities of the two proteins (Fig. 6B) and revealed that MCR-3 was more thermostable than MCR-1 ($p < 0.05$). The differences in stability with respect to thermal denaturation, with >5 °C difference in melting temperature, implied that the catalytic properties of the two proteins in mediating bacterial resistance might differ. Therefore, further investigation should focus on the association of thermodynamic stability and enzymatic function of different MCR proteins.

ACKNOWLEDGMENTS

This work was supported by the National Natural Science Foundation of China (Grant No. 31602107 and 81661138002), Capital's Funds for Health Improvement and Research (Grant No. 2018-4-3017), and Medical Research Council grant DETER-XDR-CHINA (MR/P007295/1).

CONFLICTS OF INTEREST

None.

References

1. Nation RL, Li J. 2009. Colistin in the 21st century. Curr Opin Infect Dis 22:535-43.
2. Trimble MJ, Mlynárčik P, Kolář M, Hancock REW. 2016. Polymyxin: alternative mechanisms of action and resistance. Cold Spring Harb Perspect Med 6:pii: a025288.
3. Landman D, Georgescu C, Martin DA, Quale J. 2008. Polymyxins revisited. Clin Microbiol Rev 21:449-465.
4. Poire L, Jayol A, Nordmann P. 2017. Polymyxins: antibacterial activity, susceptibility testing, and resistance mechanisms encoded by plasmids or chromosomes. Clin Microbiol Rev 30:557-596.
5. Anandan A, Evans GL, Condic-Jurkic K, O'Mara ML, John CM, Phillips NJ, Jarvis GA, Wills SS, Stubbs KA, Moraes I, Kahler CM, Vrielink A. 2017. Structure of a lipid A phosphoethanolamine transferase suggests how conformational changes govern substrate binding. Proc Natl Acad Sci U S A 114:2218-2223.
6. Liu Y-Y, Wang Y, Walsh TR, Yi L-X, Zhang R, Spencer J, Doi Y, Tian G, Dong B, Huang X, Yu L-F, Gu D, Ren H, Chen X, Lv L, He D, Zhou H, Liang Z, Liu J-H, Shen J. 2016. Emergence of plasmid-mediated colistin resistance mechanism *MCR-1* in animals and human beings in China: a microbiological and molecular biological study. Lancet Infect Dis 16:161-168.
7. Yin W, Li H, Shen Y, Liu Z, Wang S, Shen Z, Zhang R, Walsh TR, Shen J, Wang Y. 2017. Novel plasmid-mediated colistin resistance gene *mcr-3* in *Escherichia coli*. MBio 8:e00543-17.
8. Xavier BB, Lammens C, Ruhal R, Kumar-Singh S, Butaye P, Goossens H, Malhotra-Kumar S. 2016. Identification of a novel plasmid-mediated colistin-resistance gene, *mcr-2*, in *Escherichia coli*, Belgium, June 2016. Euro Surveill 21:1-6.
9. Borowiak M, Fischer J, Hammerl JA, Hendriksen RS, Szabo I, Malorny B. 2017. Identification of a novel transposon-associated phosphoethanolamine transferase gene, *mcr-5*, conferring colistin resistance in *d*-tartrate fermenting *Salmonella enterica* subsp. *enterica* serovar Paratyphi B. J Antimicrob Chemother 72:3317-3324.
10. Carattoli A, Villa L, Feudi C, Curcio L, Orsini S, Luppi A, Pezzotti G, Magistrali CF. 2017. Novel plasmid-mediated colistin resistance *mcr-4* gene in *Salmonella* and *Escherichia coli*, Italy 2013, Spain and Belgium, 2015 to 2016. Euro Surveill 22:pii:30589.
11. Litrup E, Kiil K, Hammerum AM, Roer L, Nielsen EM, Torpdahl M. 2017. Plasmid-borne colistin resistance gene *mcr-3* in *Salmonella* isolates from human infections, Denmark, 2009-17. Euro Surveill 22:pii=30587.
12. Ling Z, Yin W, Li H, Zhang Q, Wang X, Wang Z, Ke Y, Wang Y, Shen J. 2017. Chromosome-mediated *mcr-3* variants in *Aeromonas veronii* from chicken meat. Antimicrob Agents Chemother 61:pii:e01272-17.
13. Liu L, Feng Y, Zhang X, McNally A, Zong Z. 2017. A new variant of *mcr-3* in an extensively drug-resistant *Escherichia coli* clinical isolate carrying *mcr-1* and

bla$_{NDM-5}$. Antimicrob Agents Chemother 61:pii:e01757-17.

14. Roer L, Hansen F, Stegger M, Sonksen UW, Hasman H, Hammerum AM. 2017. Novel *mcr-3* variant, encoding mobile colistin resistance, in an ST131 *Escherichia coli* isolate from bloodstream infection, Denmark, 2014. Euro Surveill 22:pii=30584.
15. Wang R, van Dorp L, Shaw LP, Bradley P, Wang Q, Wang X, Jin L, Zhang Q, Liu Y, Rieux A, Dorai-Schneiders T, Weinert LA, Iqbal Z, Didelot X, Wang H, Balloux F. 2018. The global distribution and spread of the mobilized colistin resistance gene *mcr-1*. Nat Commun 9:1179.
16. Zhang J, Chen L, Wang J, Butaye P, Huang K, Qiu H, Zhang X, Gong W, Wang C. 2018. Molecular detection of colistin resistance genes (*mcr-1* to *mcr-5*) in human vaginal swabs. BMC Res Notes 11:143.
17. Del Bianco F, Morotti M, Pedna MF, Farabegoli P, Sambri V. 2018. Microbiological surveillance of plasmid mediated colistin resistance in human *Enterobacteriaceae* isolates in Romagna (Northern Italy): August 2016–July 2017. International Journal of Infectious Diseases 69:96-98.
18. Hankins JV, Madsen JA, Needham BD, Brodbelt JS, Trent MS. 2013. The outer membrane of Gram-negative bacteria: lipid A isolation and characterization. Methods Mol Biol 966:239-258.
19. Biasini M, Bienert S, Waterhouse A, Arnold K, Studer G, Schmidt T, Kiefer F, Gallo Cassarino T, Bertoni M, Bordoli L, Schwede T. 2014. SWISS-MODEL: modelling protein tertiary and quaternary structure using evolutionary information. Nucleic Acids Res 42:W252-8.
20. Eswar N. 2003. Tools for comparative protein structure modeling and analysis. Nucleic Acids Res 31:3375-3380.
21. Trott O, Olson AJ. 2010. AutoDock Vina: improving the speed and accuracy of docking with a new scoring function, efficient optimization, and multithreading. J Comput Chem 31:455-461.
22. CLSI. 2015. Performance standards for antimicrobial disk and dilution susceptibility tests for Bacteria isolated from animals: approved standard M31-A3. VET01S, 3rd ed:128.
23. Gao R, Hu Y, Li Z, Sun J, Wang Q, Lin J, Ye H, Liu F, Srinivas S, Li D, Zhu B, Liu YH, Tian GB, Feng Y. 2016. Dissemination and Mechanism for the *MCR-1* Colistin Resistance. PLoS Pathog 12:e1005957.
24. Kelesidis T, Falagas ME. 2015. The safety of polymyxin antibiotics. Expert Opin Drug Saf 14:1687-1701.
25. Hinchliffe P, Yang QE, Portal E, Young T, Li H, Tooke CL, Carvalho MJ, Paterson NG, Brem J, Niumsup PR, Tansawai U, Lei L, Li M, Shen Z, Wang Y, Schofield CJ, Mulholland AJ, Shen J, Fey N, Walsh TR, Spencer J. 2017. Insights into the Mechanistic Basis of Plasmid-Mediated Colistin Resistance from Crystal Structures of the Catalytic Domain of MCR-1. Sci Rep 7:39392-39401.
26. Stojanoski V, Sankaran B, Prasad BV, Poirel L, Nordmann P, Palzkill T. 2016. Structure of the catalytic domain of the colistin resistance enzyme MCR-1. BMC Biol 14:81-90.
27. Ma G, Zhu Y, Yu Z, Ahmad A, Zhang H. 2016. High resolution crystal structure of the

386 catalytic domain of MCR-1. Sci Rep 6:39540.
387 28. Wei P, Song G, Shi M, Zhou Y, Liu Y, Lei J, Chen P, Yin L. 2017. Substrate analog
388 interaction with MCR-1 offers insight into the rising threat of the plasmid-mediated
389 transferable colistin resistance. FASEB J 32:1-18.
390 29. Micsonai A, Wien F, Kernya L, Lee YH, Goto Y, Refregiers M, Kardos J. 2015.
391 Accurate secondary structure prediction and fold recognition for circular dichroism
392 spectroscopy. Proc Natl Acad Sci U S A 112:E3095-103.

393

394 **Figure Legends**

395 **FIG. 1 ESI-QTOF/MS analysis showing the PEA modification of bacterial lipid A**
396 **mediated by MCR-3 and MCR-1.** (A) ESI-QTOF/MS spectrum of the negative ion of lipid
397 A extracted from the recombinant control strain *E. coli* W3110 (pUC19). Lipid A had a
398 prominent peak at *m/z* 1797.10 but no peak at *m/z* 1920, indicating no PEA modification. (B)
399 ESI-QTOF/MS spectrum of the negative ion of lipid A extracted from the recombinant
400 positive control strain *E. coli* W3110 (pUC19-*mcr-1*). A PEA molecule (123 Da) was added
401 to the bisphosphorylated hexa-acylated lipid A (*m/z* = 1920; i.e., 1797 + 123). (C)
402 ESI-QTOF/MS spectrum of lipid A extracted from the recombinant strain *E. coli* W3110
403 (pUC19-*mcr-3*). The peak observed at *m/z* 1920 was consistent with the addition of a single
404 PEA group (123 Da) to ions represented by the prominent peak at *m/z* 1797.2, corresponding
405 to dephosphorylated lipid A. (D) Reaction catalyzed by MCR-3.

406 **FIG. 2 Multiple sequence alignment of MCR-3, MCR-1, and EptA conducted using**
407 **Clustal Omega (http://www.ebi.ac.uk/Tools/msa/clustalo/).**

408 **FIG. 3 Three-dimensional structure of MCR-3 generated by homology modeling.** The
409 protein was shown as a gray strip model. The catalytic residues were shown as a stick model,
410 and Zn^{2+} ions were shown by a gray sphere. The numbers in red indicated the distance
411 between coordination bonds (Å).

FIG. 4 Schematic showing the interaction between L-αPEA and the amino acids around the active site of MCR-3. (A) Hydrophobic residues were indicated by the green solid line and green residue labels, while the black dashed line represented the hydrogen bond. (B) Three-dimensional model of the binding between L-αPEA and the MCR-3 active site. The protein was shown in gray, with interacting residues shown as a green stick model, L-αPEA as a yellow stick model, and zinc ions in gray spheres, with black dotted lines indicating the interaction and distance between the L-αPEA and MCR-3 molecules.

FIG. 5 Proposed reaction mechanism of L-αPEA catalyzed by MCR-3.

FIG. 6 Secondary structure characterization of MCR-1 and MCR-3 by CD analysis. (A) Normalized CD spectra of MCR-1 and MCR-3. Data were obtained at 20 °C using 10 mM phosphate buffer, with a protein concentration of ~2.5 μM. (B) Thermal stability melting curves. Melting temperatures of MCR-1 and MCR-3 as determined by CD. MCR-1: 61.14 °C; MCR-3: 66.19 °C.

FIG. 1

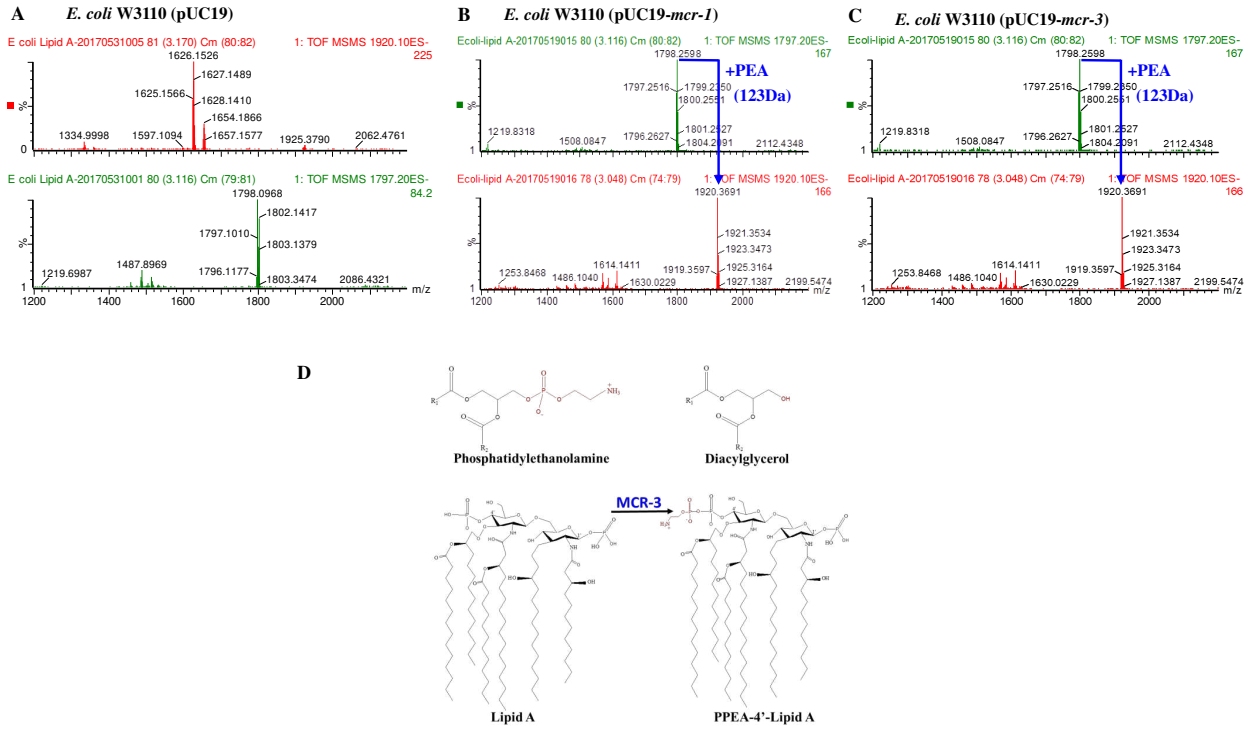

FIG. 1 ESI-QTOF/MS analysis showing the PEA modification of bacterial lipid A mediated by MCR-3 and MCR-1. (A) ESI-QTOF/MS spectrum of the negative ion of lipid A extracted from the recombinant control strain *E. coli* W3110 (pUC19). Lipid A had a prominent peak at *m/z* 1797.10 but no peak at *m/z* 1920, indicating no PEA modification. (B) ESI-QTOF/MS spectrum of the negative ion of lipid A extracted from the recombinant positive control strain *E. coli* W3110 (pUC19-*mcr-1*). A PEA molecule (123 Da) was added to the bisphosphorylated hexa-acylated lipid A (*m/z* = 1920; i.e., 1797 + 123). (C) ESI-QTOF/MS spectrum of lipid A extracted from the recombinant strain *E. coli* W3110 (pUC19-*mcr-3*). The peak observed at *m/z* 1920 was consistent with the addition of a single PEA group (123 Da) to ions represented by the prominent peak at *m/z* 1797.2, corresponding to dephosphorylated lipid A. (D) Reaction catalyzed by MCR-3.

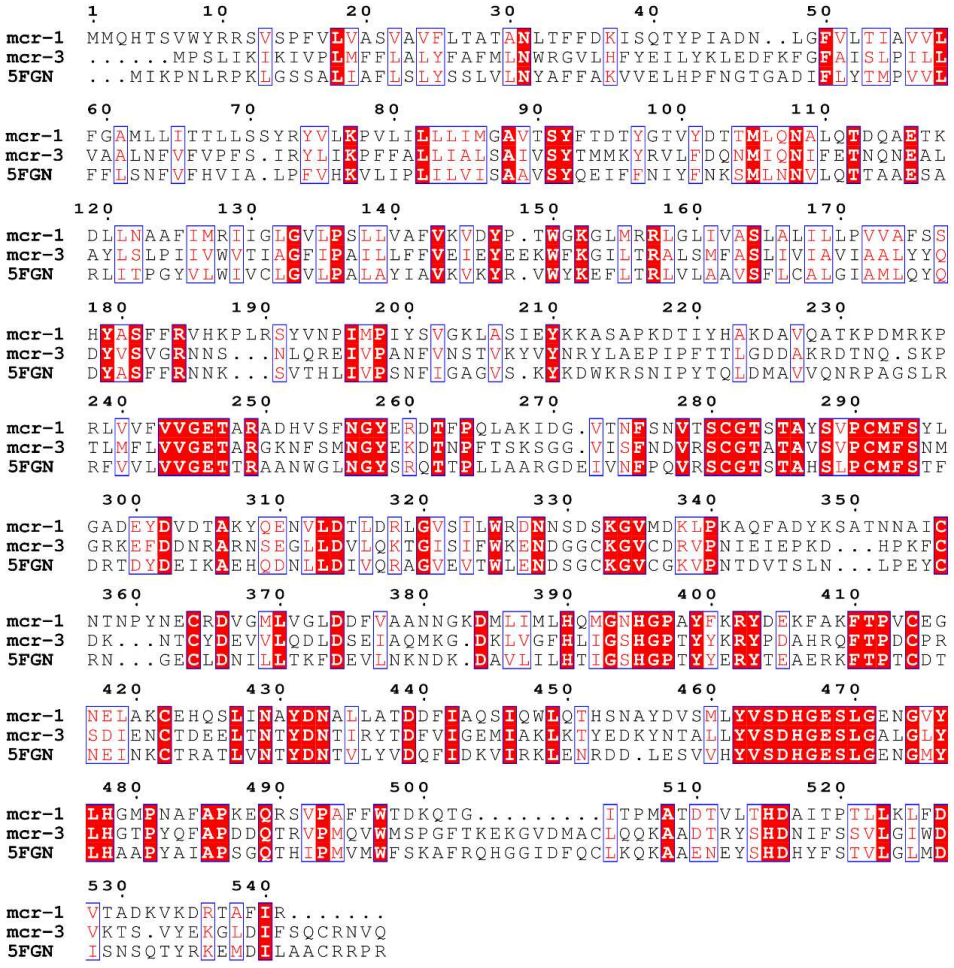

FIG. 2 Multiple sequence alignment of MCR-3, MCR-1, and EptA conducted using Clustal Omega (http://www.ebi.ac.uk/Tools/msa/clustalo/).

445 **FIG. 3**

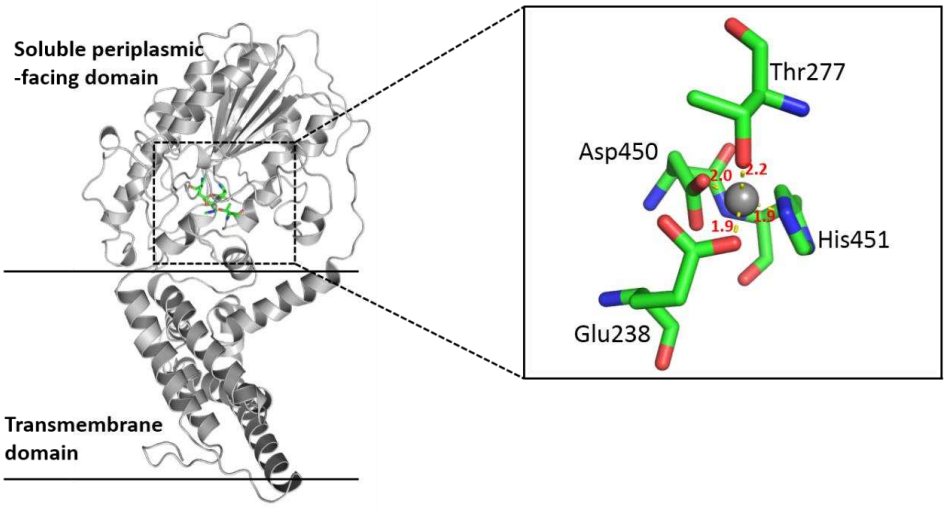

446

447 **FIG. 3 Three-dimensional structure of MCR-3 generated by homology modeling.**

448 The protein was shown as a gray strip model. The catalytic residues were shown as a

449 stick model, and Zn^{2+} ions were shown by a gray sphere. The numbers in red

450 indicated the distance between coordination bonds (Å).

451 **FIG. 4**

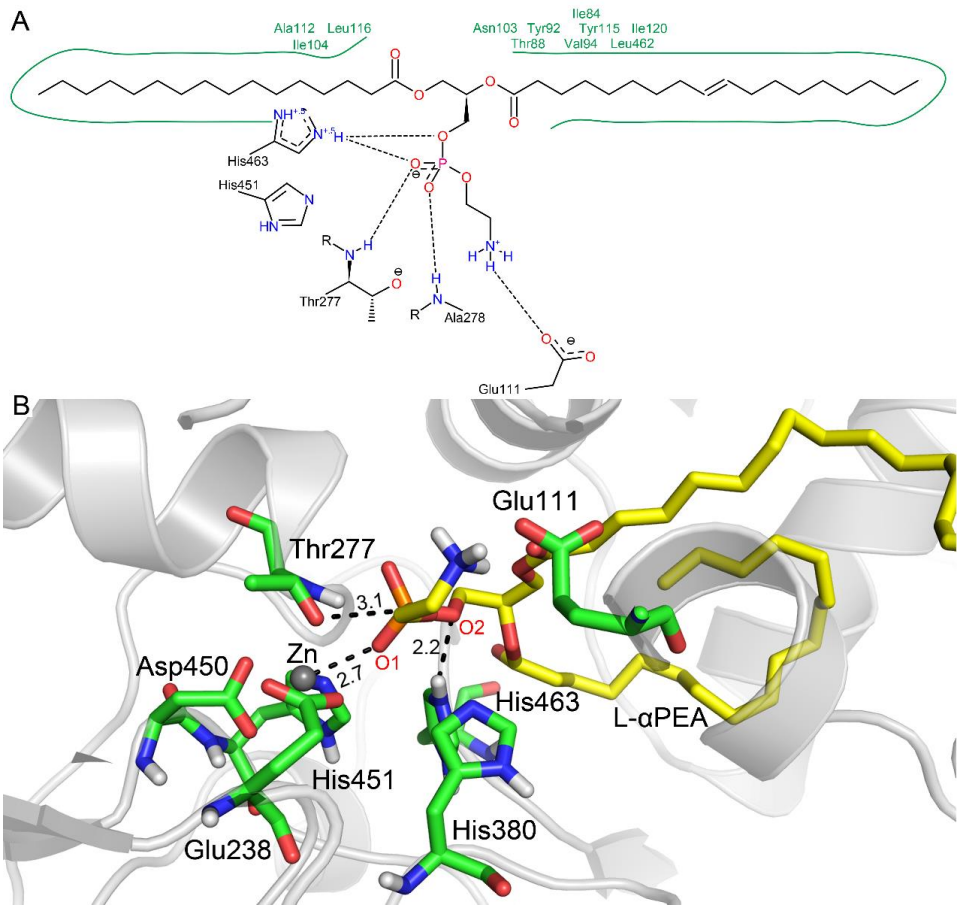

452

453 **FIG. 4 Schematic showing the interaction between L-αPEA and the amino acids**
454 **around the active site of MCR-3.** (A) Hydrophobic residues were indicated by the
455 green solid line and green residue labels, while the black dashed line represented the
456 hydrogen bond. (B) Three-dimensional model of the binding between L-αPEA and the
457 MCR-3 active site. The protein was shown in gray, with interacting residues shown as
458 a green stick model, L-αPEA as a yellow stick model, and zinc ions in gray spheres,
459 with black dotted lines indicating the interaction and distance between the L-αPEA
460 and MCR-3 molecules.

461 **FIG. 5**

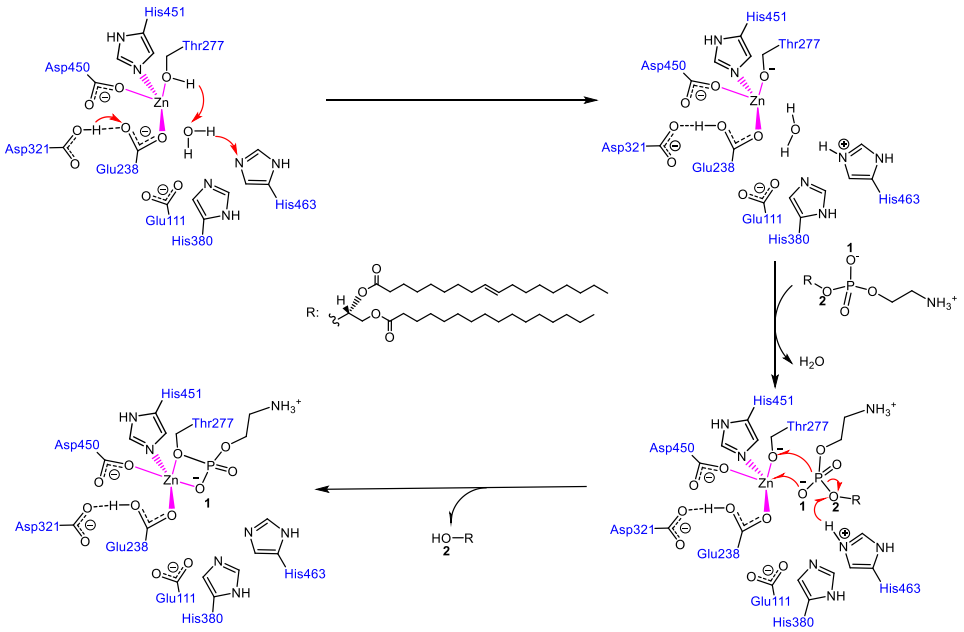

462

463 **FIG. 5 Proposed reaction mechanism of L-αPEA catalyzed by MCR-3.**

464 **FIG. 6**

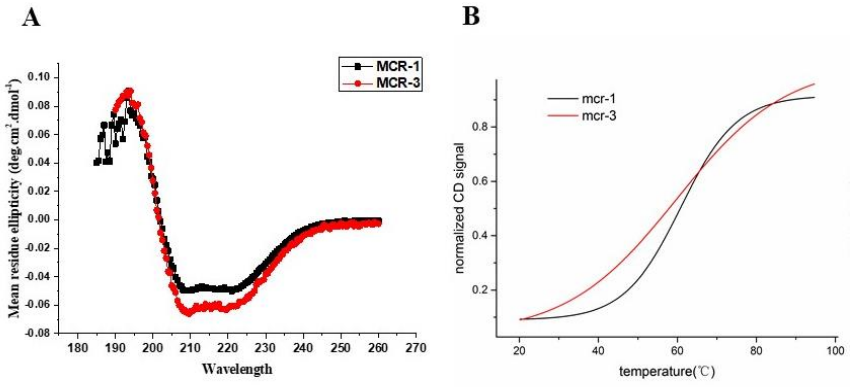

465

466 **FIG. 6 Secondary structure characterization of MCR-1 and MCR-3 by CD analysis.** (A)

467 Normalized CD spectra of MCR-1 and MCR-3. Data were obtained at 20 °C using 10 mM

468 phosphate buffer, with a protein concentration of ~2.5 μM. (B) Thermal stability melting

469 curves. Melting temperatures of MCR-1 and MCR-3 as determined by CD. MCR-1: 61.14 °C;

470 MCR-3: 66.19 °C.

471 **Tables**

472 **Table 1** Multiple sequence alignment of the selected homology templates.

	Template	Total score	E-value	Identity	Query cover	Resolution/ Å
MCR-3	5FGN	408	7e-137	39%	98%	2.75
	4KAY	310	2e-101	44%	60%	1.78
	4KAV	301	5e-98	44%	60%	1.43
	5K4P	305	6e-97	35%	70%	1.32

473 **Table 2** MIC values for colistin and polymyxin against *E. coli* strain DH5α carrying the

474 wild-type *mcr-3* gene or either of the two mutation variants (Thr277Ala and Thr277Ser).

E. coli DH5α Strains	Colistin (μg/ml)	Polymyxin (μg/ml)
DH5α	0.5	0.5
pUC19	0.5	0.5
pUC19-*mcr-3*	4	4
pUC19-*mcr-3* (Thr277Ala)	0.5	0.5
pUC19-*mcr-3* (Thr277Ser)	1	1

475

476